Applied Ocean Research 14 (1992) 201–213

Propagation and trapping of obliquely incident wave groups over a trench with currents

Philip L.-F. Liu, Yong-Sik Cho

Joseph DeFrees Hydraulics Laboratory, School of Civil and Environmental Engineering, Cornell University, Ithaca, New York 14853, USA

Jan K. Kostense & Maarten W. Dingemans

Delft Hydraulics, PO Box 152, 8300 AD Emmeloord, The Netherlands

(Received 17 June 1991; accepted 31 January 1992)

The analytical solutions of secord-order long waves generated by the diffraction of short wave groups by a combination of depth and current velocity discontinuities are presented. The incident wave groups consist of two co-linear short waves with slightly different frequencies. These incident short wave groups are reflected partially by the abrupt changes in depth and current velocity. The incident, reflected, and transmitted wave groups are accompanied by the second-order locked long waves, which propagate together with the wave envelopes of the short waves at their group velocity. Because of the discontinuity in the second-order free surface displacement of the locked long waves, free long waves are generated, which propagate at the shallow-water phase speed and in a direction different from those of short waves and wave envelopes. With certain combinations of angle of wave incidence, depth ratios and current velocity, the free long waves can be trapped in the vicinities of depth and current discontinuities. Several examples are given to illustrate the resonance of trapped free long waves.

1 INTRODUCTION

When a train of modulated wave groups propagates over a slowly varying topography and current field, two types of second-order long waves are generated due to refraction and shoaling.[1–4] The locked (forced) long waves propagate with the wave envelopes at the group velocities of the carrier (short) waves. The free long waves propagate at the shallow-water speed, $(gh)^{1/2}$, and in a direction different from those of the carrier waves and the wave envelopes. These (forced and free) long waves, although second-order quantities, play important roles in many coastal engineering problems, such as harbor resonances[5–7] and coastal processes,[8,9] if they are trapped and resonated in the nearshore area.

Agnon and Mei[10] demonstrated that the trapped long waves can indeed be excited on a long rectangular shelf. By employing asymptotic methods, Agnon and Mei[10] required the continuity of long wave potentials and the second-order normal fluxes across the edges of the shelf. Their approach leads to the continuity in the second-order free surface displacements.

In this paper the authors examine the scattering of wave groups by not only the discontinuities of depth but also the abrupt changes in current velocities. A typical physical domain representing a uniform current flowing along a trench is shown in Fig. 1. This configuration may be considered as a first approximation to tidal flow along a dredged channel. The diffraction of short waves by this configuration has been studied by Kirby *et al.*[11] In the present investigation the authors focus attention on the generation and propagation of the second-order long waves. In solving second-order long wave problems, we require the continuity of the second-order free surface displacement as well as the normal fluxes along the edges of the trench (and the discontinuity of the current velocities).

The following section summarizes the diffraction theory of the short waves. The eigenfunction expansion

Applied Ocean Research 0141-1187/92/$05.00

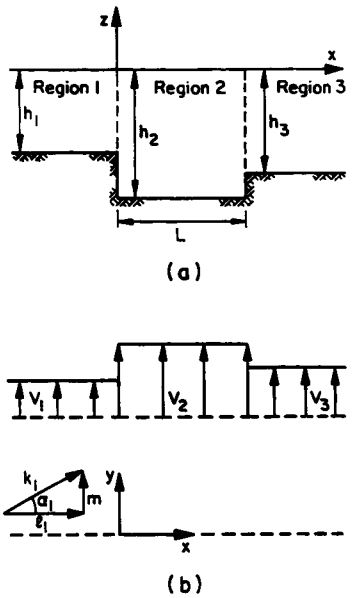

Fig. 1. Definition sketch.

method is used[11,12] and the effects of evanescent modes are included. In Section 3, the solutions of the locked and the free long waves are presented. The possibility of the resonance of trapped free long waves over a shelf with currents is discussed. Several numerical examples are given in Section 4.

2 FORMULATION OF THE PROBLEM

The diffraction of slowly modulated bichromatic water waves by depth and current variations is considered. As shown in Fig. 1, the abrupt changes in current velocity coincide with those in depth variations and both are uniform in y-direction.

2.1 Incident wave groups

The incident wave groups are the superposition of two co-linear monochromatic waves of slightly different frequencies, $\omega_0 \pm \epsilon\Omega_0$, where $\epsilon \ll 1$ is a small parameter and is assumed to be in the same order of magnitude as the wave slope of the carrier waves. The leading incident wave potential, Φ_I, and the associated free surface displacement, ζ_I, can be written as:

$$\Phi_I(x,y,z,t) = -\frac{igA_I}{2\sigma_1}\frac{\cosh k_1(z+h_1)}{\cosh k_1 h_1} \times \exp[i(l_1 x + my - \omega_0 t)] + * \quad (1)$$

$$\zeta_I(x,y,t) = \tfrac{1}{2}A_I \exp[i(l_1 x + my - \omega_0 t)] + * \quad (2)$$

where $*$ denotes the complex conjugate of the prededing term, $\boldsymbol{k}_1 = (l_1, m)$ and $k_1 = (l_1^2 + m^2)^{1/2}$ are the carrier wavenumber vector and its magnitude, respectively, and σ_1 is the intrinsic frequency which can be determined from the linear dispersion relation:

$$\sigma_1 = \omega_0 - mV_1 = (gk_1 \tanh k_1 h_1)^{1/2} \quad (3)$$

with V_1 and h_1 being current velocity and depth in the region $1(x < 0$, see Fig. 1). Denoting $k_1 + \epsilon K_{11}$ and $k_1 - \epsilon K_{12}$ as the wavenumber vectors for the short wave components, the wave envelope A_I of the incident wave groups can be expressed as:

$$A_I = a_0\{\exp[i(\mathbf{K}_{11}\cdot\mathbf{X} - \Omega_0 T)] + b \times \exp[-i(\mathbf{K}_{12} - \mathbf{K}_{11})\cdot\mathbf{X}]\exp[-i(\mathbf{K}_{11}\cdot\mathbf{X} - \Omega_0 T)]\}$$

where a_0 and $a_0 b$ are the amplitudes of the short wave components with the frequencies $\omega_0 \pm \epsilon\Omega_0$, respectively. In the above equation the slow variables

$$\mathbf{X} = (X, Y) = \epsilon x, \quad T = \epsilon t, \quad L_1 = \epsilon L \quad (4)$$

have been employed. From the dispersion relation (3) we can show that $0(|\mathbf{K}_{12} - \mathbf{K}_{11}|) = 0(\epsilon)$. The modulation length scale for $\exp[-i(\mathbf{K}_{12} - \mathbf{K}_{11})\cdot\mathbf{X}]$ is of $0(\epsilon^{-2})$, and, therefore, this term can be considered as unity. Replacing $\mathbf{K}_{11}$ by $\mathbf{K}_1$, the wave envelope A_I can be approximated as:

$$A_I = a_0\{\exp[i(\mathbf{K}_1\cdot\mathbf{X} - \Omega_0 T)] + b \times \exp[-i(\mathbf{K}_1\mathbf{X} - \Omega_0 T)]\} \quad (5)$$

The incident wave envelope is assumed to be co-linear with the carrier waves, and the wavenumber vector of the wave envelope, $\mathbf{K}_1$, is parallel to the wavenumber of the carrier waves, $\mathbf{k}_1$. Denoting the angle of incidence as α_1, we can define the wavenumber components in the following forms:

$$K_{1x} = K_1\cos\alpha_1, \quad K_{1y} = K_1\sin\alpha_1, \quad K_1 = |\mathbf{K}_1|,$$
$$l_1 = k_1\cos\alpha_1, \quad m = k_1\sin\alpha_1, \quad k_1 = |\mathbf{k}_1| \quad (6)$$

The wave envelope must satisfy the wave action equation:[4]

$$\frac{\partial|A_I|^2}{\partial T} + (\mathbf{Cg}_1 + \mathbf{V}_1)\cdot\nabla|A_I|^2 = 0, \quad \mathbf{Cg}_1 = \frac{d\sigma_1}{dk_1}\frac{\mathbf{k}_1}{k_1} \quad (7)$$

in which $\nabla = (\partial/\partial X, \partial/\partial Y)$, and Ω_0 is related to K_1, i.e.

$$\Omega_0 = (\mathbf{Cg}_1 + \mathbf{V}_1)\cdot\mathbf{K}_1 \quad (8)$$

Because $\mathbf{Cg}_1$ is determined from eqns (3) and (7), one can choose a value for either K_1 or Ω_0 as the detuning parameter. For convenience, we use $K_1 = k_1$ in the present study.

2.2 Diffraction of short waves

The diffraction of the incident carrier (monochromatic) waves by a trench (or a shelf) with currents (Fig. 1) has been studied by Kirby *et al.*[11] Their solution procedure is summarized here for completeness. For a monochromatic incident wave train with a

frequency $\hat{\omega}_0 (= \omega_0 \pm \epsilon\Omega_0)$, the velocity potentials within each region, $j = 1, 2, 3$ (see Fig. 1), are expressed in terms of a complete set of eigenfunctions in the following forms:

$$\Phi_j(x,y,z,t) = \left\{ A_j^{\pm} \exp(\pm \mathrm{i}\hat{l}_j x) f_{j,0}(z) + \sum_{n=1}^{\infty} B_{j,n}^{\pm} \exp(\pm \hat{\lambda}_{j,n} x) f_{j,n}(z) \right\} \times \exp[\mathrm{i}(\hat{m}y - \hat{\omega}_0 t)] \qquad (j = 1,2,3) \tag{9}$$

in which:

$$f_{j,0}(z) = \cosh \hat{k}_j(z + h_j) \tag{10a}$$

$$f_{j,n}(z) = \cos[\hat{K}_{j,n}(z + h_j)] \tag{10b}$$

with $\hat{k}_j$ being the real root of

$$\hat{\sigma}_j = \hat{\omega}_0 - \hat{m}V_j = (g\hat{k}_j \tanh \hat{k}_j h_j)^{1/2} \tag{11}$$

and $\hat{K}_{j,n}$ being the real roots of

$$\hat{\sigma}_j = \hat{\omega}_0 - \hat{m}V_j = (-g\hat{K}_{j,n} \tan \hat{K}_{j,n} h_j)^{1/2} \tag{12}$$

In eqn (9) the first term denotes the right- and left-propagating wave components and the second term represents the sum of all evanescent modes. The wavenumber components $\hat{l}_j$ and $\hat{\lambda}_{j,n}$ are related to the eigenvalues $\hat{k}_j$ and $\hat{K}_{j,n}$ as follows:

$$\hat{l}_j = (\hat{k}_j^2 - \hat{m}^2)^{1/2} = \hat{k}_j \cos \alpha_j, \qquad \hat{m} = \hat{k}_j \sin \alpha_j,$$
$$\hat{\lambda}_{j,n} = (\hat{K}_{j,n}^2 + \hat{m}^2)^{1/2} \tag{13}$$

Evans[12] and Kirby *et al.*[11] have presented a set of matching conditions along the edges of the depth (and/or current) discontinuities, which leads to the solutions for $A_j^{\pm}$ and $B_{j,n}^{\pm}$ in terms of the incident potential A_1^+. The details of the matching conditions will not be repeated here.

Once the unknown coefficients $A_j^{\pm}$ and $B_{j,n}^{\pm}$ are obtained, the first-order wave field for the monochromatic waves is determined. For later use, the authors define the following functions in each region:

$$a_j = 2\mathrm{i}\frac{\hat{\sigma}_j}{g} \cosh \hat{k}_j h_j \qquad (j = 1,2,3) \tag{14}$$

Setting A_1^+ to be unity, we can define:

$$\begin{aligned} R_1 &= A_1^-, & T_1 &= 1 \\ R_2 &= \frac{a_2}{a_1} A_2^-, & T_2 &= \frac{a_2}{a_1} A_2^+ \\ R_3 &= 0, & T_3 &= \frac{a_3}{a_1} A_3^+ \end{aligned} \tag{15}$$

in which R_1 denotes the reflection coefficient and T_3 represents the transmission coefficient of the trench-current system. Because the above equations are functions of frequency, R_j and T_j take different values at $\omega_0 \pm \epsilon\Omega_0$. Thus:

$$R_j^+ = R_j(\omega_0 + \epsilon\Omega_0) \tag{16a}$$

$$R_j^- = bR_j(\omega_0 - \epsilon\Omega_0) \tag{16b}$$

$$T_j^+ = T_j(\omega_0 + \epsilon\Omega_0) \tag{17a}$$

$$T_j^- = bT_j(\omega_0 - \epsilon\Omega_0) \tag{17b}$$

where R_j^+ denotes the value of R_j evaluated at $\omega + \epsilon\Omega_0$, etc.

It should be pointed out that the analysis given above breaks down when caustics appear in either region 2 or region 3. In such cases, the wavenumber component in the x-direction, $\hat{l}_j$ ($j = 2$ or 3), becomes zero. The corresponding critical incident wave angle is:

$$\alpha_1^{\mathrm{cr}} = \arcsin\left(\frac{\hat{k}_j}{\hat{k}_1}\right) \qquad (j = 2 \text{ or } 3) \tag{18}$$

The present study excludes the caustics.

2.3 Wave envelopes of propagation modes

Once the wave amplitudes for each region are determined for the carrier waves, the corresponding wave envelopes can be readily obtained by superposition. The incident wave envelope has already been given in eqn (5) and is rewritten as:

$$A_{\mathrm{I}} = a_0\{\exp[\mathrm{i}(K_{1x}X + K_{1y}Y - \Omega_0 T)] + b\exp[-\mathrm{i}(K_{1x}X + K_{1y}Y - \Omega_0 T)]\} \tag{19}$$

in which eqn (6) has been used. The left-propagating and the right-propagating wave groups can be viewed as the superposition of two monochromatic waves with slightly different frequencies, $\hat{\omega}_0 = \omega_0 \pm \epsilon\Omega_0$. Thus, the leading potential and free surface displacement of the left-propagating ($-x$-direction) wave group can be expressed as:

$$\Phi_R^j(x,y,z,t) = A_R^j f_j(z) \exp[\mathrm{i}(-l_j x + my - \omega_0 t)] + * \tag{20a}$$

$$\zeta_R^j(x,y,t) = \tfrac{1}{2} A_R^j \exp[\mathrm{i}(-l_j x + my - \omega_0 t)] + * \tag{20b}$$

where:

$$f_j(z) = -\frac{\mathrm{i}g}{2\sigma_j} \frac{\cosh k_j(z + h_j)}{\cosh k_j h_j} \tag{21}$$

$$A_R^j = a_0 R_j^{\pm} \exp[\pm \mathrm{i}(-K_{jx}X + K_{jy}Y - \Omega_0 T)] \tag{22}$$

in which summation over + and − is implied. Similarly, the velocity potential and the free surface displacement for the right-propagating (+ x-direction) wave group

can be expressed as:

$$\Phi_T^j(x,y,z,t) = A_T^j f_j(z) \exp[\mathrm{i}(l_j x + my - \omega_0 t)] + * \tag{23a}$$

$$\zeta_T^j(x,y,t) = \tfrac{1}{2} A_T^j \exp[\mathrm{i}(l_j x + my - \omega_0 t)] + * \tag{23b}$$

where:

$$A_T^j = a_0 T_j^{\pm} \exp[\pm \mathrm{i}(K_{jx}X + K_{jy}Y - \Omega_0 T)] \tag{24}$$

Similar to eqn (8) the frequency of the wave envelope, Ω_0, is related to the wavenumbers in each region, i.e.:

$$\Omega_0 = \mathbf{K}_1 \cdot (\mathbf{C}g_1 + \mathbf{V}_1) = \mathbf{K}_2 \cdot (\mathbf{C}g_2 + \mathbf{V}_2) = \mathbf{K}_3 \cdot (\mathbf{C}g_3 + \mathbf{V}_3) \tag{25a}$$

where:

$$\mathbf{C}g_j = \frac{\mathrm{d}\sigma_j}{\mathrm{d}k_j}\frac{\mathbf{k}_j}{k_j} \qquad (j = 1,2,3) \tag{25b}$$

is the group velocity vector in the jth region and σ_j is defined in eqn (11). Denoting α_j ($j = 1,2,3$) as the angle of the carrier wave propagation in the jth region, we can rewrite eqn (25) in the following form:

$$\Omega_0 = K_{jx} Cg_j \cos\alpha_j + K_{jy}(Cg_j \sin\alpha_j + V_j) \quad (j = 1,2,3) \tag{26}$$

in which $K_{jy} = K_{1y}$. Substituting eqn (13) into eqn (26), we obtain:

$$K_{jx} = \frac{k_j}{l_j Cg_j}\sum_j - K_{1y}\frac{m}{l_j} = l_j + \frac{k_j^2}{l_j}\left(\frac{\sum_j}{k_j Cg_j} - 1\right) \tag{27}$$

where

$$\sum_j = \Omega_0 - K_{1y} V_j \tag{28}$$

may be viewed as the intrinsic frequency of the wave envelope. Similar results have been obtained by Liu *et al.*[4] for the refraction of wave groups over a shear current.

As pointed out by Liu *et al.*,[4] the wave envelope can also experience caustics in region 2 or region 3 for a certain combination of angle of wave incidence, depth and current speed. When caustics appear, $K_{jx} = 0$ ($j = 2$ or 3). From eqn (27), we can find the critical angle of incidence for the appearance of caustics in wave envelope to be:

$$\bar{\alpha}_1^{\mathrm{cr}} = \arcsin\left\{\frac{k_j V_j}{2k_1 Cg_j}\left[-1 + \left(1 + \frac{4k_1 Cg_1 Cg_j}{k_j V_j^2}\right)^{1/2}\right]\right\} \tag{29}$$

which is different from α_1^{cr}, the critical angle of incidence for the short wave (carrier) caustics.

3. LOCKED AND FREE LONG WAVES

The governing equations for the second-order long waves induced by the refraction and diffraction of wave groups have been derived by many researchers (e.g. Refs 4 and 13). It has been shown that over a region of constant depth and constant current velocity, the locked long waves are generated only by the self-product of plane short wave components (e.g. Ref. 10). Therefore, in the present problem the evanescent modes of the carrier waves, which decay exponentially away from the edges of the trench, do not contribute to the generation of long waves. Denoting Ψ_i^j ($i = R$, T and $j = 1,2,3$) as the potential of the long waves associated with the left- ($i = R$) and right- ($i = T$) propagating wave groups in the jth region, the governing equations for the second-order long waves are:[4,14]

$$\frac{\partial \xi_i^j}{\partial T} + \nabla\cdot\left[\xi_i^j \mathbf{V}_j + h_j \nabla\Psi_i^j \pm \mathbf{k}_j \frac{g|A_i^j|^2}{2\sigma_j}\right] = 0 \tag{30}$$

$$\xi_i^j = -\frac{1}{g}\left(\frac{\partial}{\partial T} + V_j\frac{\partial}{\partial Y}\right)\Psi_i^j - \frac{\sigma_j^2 |A_i^j|^2}{4g\sinh^2 k_j h_j} \tag{31}$$

where ξ_i^j denotes the second-order mean free surface displacement associated with the long waves Ψ_i^j. In eqns (30) and (31), A_i^j represents the modulated wave amplitude for each propagating wave group, and the positive sign in front of the last term in eqn (30) is used for $i = T$ and the negative sign for $i = R$. Equation (30) represents the depth-averaged continuity equation for each long wave component; the last term in the equation denotes the 'Stokes' drift' caused by the wave groups. In each region ξ_i^j can be eliminated from eqns (30) and (31) to yield an equation for Ψ_1^j. Thus:

$$\left(\frac{\partial}{\partial T} + V_j\frac{\partial}{\partial Y}\right)^2 \Psi_i^j - gh_j\left(\frac{\partial^2}{\partial X^2} + \frac{\partial^2}{\partial Y^2}\right)\Psi_i^j = \frac{g^2}{2}\nabla\cdot\left(\mathbf{k}_j\frac{|A_i^j|^2}{\sigma_j}\right) - \frac{gk_j}{2\sinh 2k_j h_j} \times \left(\frac{\partial |A_i^j|^2}{\partial T} + V_j\frac{\partial |A_i^j|^2}{\partial Y}\right) \tag{32}$$

Introducing the dimensionless variables:

$$\mathbf{X} \to \frac{\mathbf{X}}{k_\infty}, \quad T \to \frac{T}{\omega_0}, \quad \sigma \to \omega_0\sigma, \quad h \to \frac{h}{k_\infty}, \quad k \to k_\infty k, \quad Cg \to \frac{Cg\omega_0}{k_\infty}, \quad \Psi \to (2a_0)^2\omega_0\Psi, \quad \xi \to (2a_0)^2 k_\infty \xi, \quad \mathbf{V} \to \frac{\mathbf{V}\omega_0}{k_\infty}, \quad A \to a_0 A \tag{33}$$

in which a_0 denotes the incident wave amplitude and $k_\infty = \omega_0^2/g$; and substituting eqns (22) and (24) into eqn (32), we obtain a set of dimensionless governing equations for the long waves:

$$\left(\frac{\partial}{\partial T}+V_j\frac{\partial}{\partial Y}\right)^2\Psi_i^j-h_j\left(\frac{\partial^2}{\partial X^2}+\frac{\partial^2}{\partial Y^2}\right)\Psi_i^j$$
$$=\frac{1}{4}ik_j|A_i^j|^2\sum_j\left(\frac{1}{\sinh 2k_jh_j}+\frac{1}{\sigma_jCg_j}\right)$$
$$\times\exp\left[2i(\pm K_{jx}X+K_{1y}Y-\Omega_0T)\right]+* \qquad (34)$$

where the positive sign is used in the argument of the exponential function for $i=T$, while the negative sign is used for $i=R$ and $*$ denotes the complex conjugate. The solutions for eqn (34) can be decomposed into the steady-state component, Ψ_i^{js} and the dynamic component, i.e.:

$$\Psi_i^j=\Psi_i^{js}+\tfrac{1}{2}\psi_i^j(X)\exp\left[2i(K_{1y}Y-\Omega_0T)\right]+* \qquad (35)$$

The steady-state components do not contribute to the mean free surface displacement ξ_i^j. From eqn (36) the amplitude function of the dynamic component satisfies the following equation:

$$\left[\frac{d^2}{dX^2}+\frac{4}{h_j}\left(\sum_j^2-K_{1y}^2h_j\right)\right]\psi_i^j=-\frac{1}{2h_j}ik_j|A_i^j|^2$$
$$\times\sum_j\left(\frac{1}{\sinh 2k_jh_j}+\frac{1}{\sigma_jCg_j}\right)\exp\left[\pm 2iK_{jx}X\right] \qquad (36)$$

3.1 Locked long waves

The solutions of eqn (36) consist of the particular solution (locked long waves) and the homogeneous solution (free long waves). The locked long waves in each region can be readily obtained. The locked long waves associated with the right-propagating wave groups can be expressed as:

$$(\psi_T^j)_L=-\frac{ik_j\sum_j T_j^+T_j^{-*}}{8\left(\sum_j^2-K_j^2h_j\right)}\left(\frac{1}{\sinh 2k_jh_j}+\frac{1}{\sigma_jCg_j}\right)$$
$$\times\exp\left[2iK_{jx}X\right] \qquad (37)$$

in which $*$ denotes the complex conjugate. Similarly, the locked long waves associated with the left-propagating wave groups in the jth region can be written as:

$$(\psi_R^j)_L=-\frac{ik_j\sum_j R_j^+R_j^{-*}}{8\left(\sum_j^2-K_j^2h_j\right)}\left(\frac{1}{\sinh 2k_jh_j}+\frac{1}{\sigma_jCg_j}\right)$$
$$\times\exp\left[-2iK_{jx}X\right] \qquad (38)$$

The corresponding second-order free surface displacements for the locked long waves can be calculated from eqn (31). Thus, for the left-propagating locked long waves the free surface displacement reads:

$$\xi_R^j=\tfrac{1}{2}\tilde{\xi}_R^j\exp\left[2i(K_{1y}Y-\Omega_0T)\right]$$
$$-\frac{(|R_j^+|^2+|R_j^-|^2)\sigma_j^2}{16\sinh^2 sk_jh_j}+* \qquad (39a)$$

where:

$$\tilde{\xi}_R^j=\frac{R_j^+R_j^{-*}}{4\left(\sum_j^2-K_j^2h_j\right)}\left(\frac{K_j^2h_j\sigma_j^2}{2\sinh^2 k_jh_j}+\frac{\sum_j^2 k_j}{\sigma_jCg_j}\right)$$
$$\times\exp\left(-2iK_{jx}X\right) \qquad (39b)$$

and the second term on the right-hand side of eqn (39a) represents the steady-state mean free surface set-down. The second-order free surface displacements associated with the right-propagating locked long waves can be written as:

$$\xi_T^j=\tfrac{1}{2}\tilde{\xi}_T^j\exp\left[2i(K_{1y}Y-\Omega_0T)\right]$$
$$-\frac{(|T_j^+|^2+|T_j^-|^2)\sigma_j^2}{16\sinh^2 k_jh_j}+* \qquad (40a)$$

where:

$$\tilde{\xi}_T^j=\frac{T_j^+T_j^{-*}}{4\left(\sum_j^2-K_j^2h_j\right)}\left(\frac{K_j^2h_j\sigma_j^2}{2\sinh^2 k_jh_j}+\frac{\sum_j^2 k_j}{\sigma_jCg_j}\right)$$
$$\times\exp(2iK_{jx}X) \qquad (40b)$$

It is clear that the second-order free surface displacements associated with the locked long waves are discontinuous along the edges of depth and current discontinuities. Free long wave components, which are the homogeneous solutions of eqn (36), must be added in each region. In this paper the steady-state free surface displacement is not investigated.

3.2 Free long waves

Denoting ψ_i^F ($i=R,T,D$ and E) as the outgoing free long waves in region 1 ($i=R$) and in region 3 ($i=T$), as well as the right-going ($i=D$) and the left-going ($i=E$) free long waves in region 2, the free long wave potentials are the homogeneous solutions of eqn (36), i.e.:

$$\left[\frac{d^2}{dX^2}+\frac{4}{h_j}\left(\sum_j^2-K_{1y}^2h_j\right)\right]\psi_i^F=0 \qquad (41)$$

where $j=1$ when $i=R$; $j=2$ when $i=D$ and E; and $j=3$ when $i=T$. Thus, in region 1 the free long wave

solution can be written as:

$$\psi_R^F = E_1 \exp(-2i\lambda_1 X), \quad \lambda_1 = \left(\sum_1^2 \frac{1}{h_1} - K_1{}^2 y \right)^{1/2} \tag{42}$$

where λ_1 could be either a real or an imaginary value. When λ_1 is a real value, ψ_R^F is a propagating wave. On the other hand, when λ_1 is an imaginary constant, ψ_R^F becomes an evanescent mode which decays exponentially for large negative X. The amplitude of the free long wave, E_1, is to be determined. When λ_1 is equal to zero, ψ_R^F, which is the solution of eqn (41), is the sum of a linear function in X and a constant. To avoid an unbounded solution, ψ_R^F is a constant when λ_1 becomes zero. Therefore, eqn (42) includes the case $\lambda_1 = 0$.

Similarly, the free long wave components in region 2 can be written as:

$$\psi_2^F = \psi_D^F + \psi_E^F \tag{43}$$

where:

$$\psi_D^F = E_2 \exp(2i\lambda_2 X), \quad \psi_E^F = E_3 \exp(-2i\lambda_2 X) \tag{44}$$

with:

$$\lambda_2 = \left(\sum_2^2 \frac{1}{h_2} - K_{1y}^2 \right)^{1/2} \tag{45}$$

which could be either real or imaginary. When λ_2 is zero, the free long wave solution of eqn (41) becomes:

$$\psi_2^F = \psi_D^F + \psi_E^F = C_1 X + C_2 \tag{46}$$

which remains finite within the region $2, 0 < X < L_1$. Note that eqn (46) cannot be obtained by setting λ_2 to zero in eqns (43) and (44). However, as λ_2 approaches zero, eqns (43) and (44) can be expanded in Taylor's series for small $\lambda_2 L_1 \ll 1$:

$$\psi_2^F = \psi_D^F + \psi_E^F \sim 2i\lambda_2 (E_2 - E_3) X + (E_2 + E_3) \tag{47}$$

Comparing eqns (46) and (47), we obtain:

$$C_1 = 2i\lambda_2 (E_2 - E_3), \quad C_2 = (E_2 + E_3) \tag{48}$$

This implies that when λ_2 is zero, E_2 and E_3 must be proportional to λ_2^{-1} so that C_1 remains finite. This point is discussed further in the next section.

In region 3, the free long waves are:

$$\psi_T^F = E_4 \exp(2i\lambda_3 X) \tag{49}$$

with:

$$\lambda_3 = \left(\sum_3^2 \frac{1}{h_3} - K_{1y}^2 \right)^{1/2} \tag{50}$$

When λ_3 is a real constant, the free long waves propagate in the positive X-direction. If λ_3 is an imaginary constant, ψ_T^F represents an evanescent mode which decays exponentially for large X. When λ_3 is zero, the free long wave potential becomes a constant.

The corresponding second-order free surface displacement of the free long waves can be found from eqn (31) as:

$$\tilde{\xi}_R^F = 2i \sum_1 \psi_R^F, \quad \tilde{\xi}_D^F = 2i \sum_2 \psi_D^F, \quad \tilde{\xi}_E^F = 2i \sum_2 \psi_E^F$$
$$\text{and } \tilde{\xi}_T^F = 2i \sum_3 \psi_T^F \tag{51}$$

3.3 Matching conditions

To determine the amplitudes of free long waves, matching conditions for the second-order wave solutions along the edges between regions, $X = 0$ and L_1 (see Fig. 1), must be specified. The full expression of the second-order free surface displacement near the depth and/or current discontinuity is:

$$\tilde{\xi}^L = -\frac{1}{g}\left(\frac{\partial}{\partial T} + V\frac{\partial}{\partial Y}\right)\Psi - \frac{1}{g}\left[\left|\frac{\partial \Phi}{\partial x}\right|^2 + \left|\frac{\partial \Phi}{\partial y}\right|^2 + \left|\frac{\partial \Phi}{\partial z}\right|^2 - \left(\frac{\sigma^2}{g}\Phi\frac{\partial \Phi^*}{\partial z} + *\right)\right] \qquad (z = 0)$$

where Φ denotes the first-order velocity potential and $\Psi$the second-order long wave potential. If the current is absent, the quadratic terms on the right-hand side of the above equation are continuous across the edge of the trench. The continuity of the second-order long wave potential leads to the continuity of the second-order free surface displacement. In the present problem, the current and the first-order velocity potential are discontinuous at the edge of the trench. The first matching condition requires the continuity of the second-order free surface displacement at $X = 0$ and L_1, i.e.

$$\tilde{\xi}_T^1 + \tilde{\xi}_R^1 + \tilde{\xi}_1^L + \tilde{\xi}_R^F = \tilde{\xi}_T^2 + \tilde{\xi}_R^2 + \tilde{\xi}_2^L + \tilde{\xi}_D^F + \tilde{\xi}_E^F \quad \text{at } X = 0 \tag{52a}$$

$$\tilde{\xi}_T^3 + \tilde{\xi}_3^L + \tilde{\xi}_T^F = \tilde{\xi}_T^2 + \tilde{\xi}_R^2 + \tilde{\xi}_2^L + \tilde{\xi}_D^F + \tilde{\xi}_E^F \quad \text{at } X = L_1 \tag{52b}$$

where:

$$\tilde{\xi}_j^L = -\frac{1}{g}\left[\overline{\left|\frac{\partial \Phi_j}{\partial x}\right|^2 + \left|\frac{\partial \Phi_j}{\partial y}\right|^2 + \left|\frac{\partial \Phi_j}{\partial z}\right|^2 - \left(\frac{\sigma_j^2}{g}\Phi_j\frac{\partial \Phi_j^*}{\partial z} + *\right)}\right]_{z=0}$$

in which the overbar distinguishes the terms including fast variables and $j = 1$, 2 and 3. The second matching condition requires the continuity of the second-order flux across $X = 0$ and L_1. From eqn (30) the flux in the X-direction for each wave group component can be

calculated from:

$$\frac{1}{\Sigma_j}\left[h_j\frac{\partial\psi_i}{\partial X}\pm\frac{l_j|A_i|^2}{8\sigma_j}\right]$$

Summing up the contributions from all wave group components on each side of the interfaces between regions, we obtain:

$$\frac{1}{\Sigma_1}\left[h_1\left(\frac{\partial\psi_T^1}{\partial X}+\frac{\partial\psi_R^1}{\partial X}+\frac{\partial\psi_R^F}{\partial X}\right)+\frac{l_1}{8\sigma_1}(b-R_1^+R_1^{-*})\right]$$
$$=\frac{1}{\Sigma_2}\left[h_2\left(\frac{\partial\psi_T^1}{\partial X}+\frac{\partial\psi_R^1}{\partial X}+\frac{\partial\psi_D^F}{\partial X}+\frac{\partial\psi_E^F}{\partial X}\right)\right.$$
$$\left.+\frac{l_2}{8\sigma_2}(T_2^+T_2^{-*}-R_2^+R_2^{-*})\right]\text{ at }X=0 \qquad (53a)$$

$$\frac{1}{\Sigma_3}\left[h_3\left(\frac{\partial\psi_T^3}{\partial X}+\frac{\partial\psi_T^F}{\partial X}\right)+\frac{l_3T_3^+T_3^{-*}}{8\sigma_3}\right]$$
$$=\frac{1}{\Sigma_2}\left[h_2\left(\frac{\partial\psi_T^2}{\partial X}+\frac{\partial\psi_R^2}{\partial X}+\frac{\partial\psi_D^F}{\partial X}+\frac{\partial\psi_E^F}{\partial X}\right)\right.$$
$$\left.+\frac{l_2}{8\sigma_2}(T_2^+T_2^{-*}-R_2^+R_2^{-*})\right]\text{ at }X=L_1 \qquad (53b)$$

We remark here that the matching conditions (53) for the normal flux can be reduced to the same form as those used by Agnon and Mei,[10] when the current velocity vanishes. Agnon and Mei[10] matched the second-order long wave potentials along the edges between regions, $X=0$ and L_1. From eqn (31) the dynamic components of the second-order free surface displacements in their solutions are discontinuous across the edges. On the other hand, we match the free-surface displacements associated with long waves, but allow a jump in the second-order potentials. The authors matching conditions are justified, because the velocity field and the pressure field will not be altered by introducing an arbitrary constant into the potential function.

For the cases where λ_2 is not equal to zero, we substitute the long wave solutions, eqns (37)–(40)), (42), (44) and (49), into the matching conditions (52) and (53), to obtain a set of linear algebraic equations for the amplitudes of free long waves, E_1, E_2, E_3 and E_4:

$$\mathbf{N}\begin{Bmatrix}E_1\\E_2\\E_3\\E_4\end{Bmatrix}=\begin{Bmatrix}F_1\\F_2\\F_3\\F_4\end{Bmatrix} \qquad (54)$$

where the matrix $\mathbf{N}$ is given by:

$$\mathbf{N}=\begin{Bmatrix}\Sigma_1 & -\Sigma_2 & -\Sigma_2 & 0\\ 0 & \Sigma_2e^{2i\lambda_2L_1} & \Sigma_2e^{-2i\lambda_2L_1} & -\Sigma_3e^{2i\lambda_3L_1}\\ -\dfrac{\lambda_1h_1}{\Sigma_1} & -\dfrac{\lambda_2h_2}{\Sigma_2} & \dfrac{\lambda_2h_2}{\Sigma_2} & 0\\ 0 & \dfrac{\lambda_2h_2}{\Sigma_2}e^{2i\lambda_2L_1} & -\dfrac{\lambda_2h_2}{\Sigma_2}e^{-2i\lambda_2L_1} & \dfrac{\lambda_3h_3}{\Sigma_3}e^{2i\lambda_3L_1}\end{Bmatrix} \qquad (55)$$

and the right-hand side terms of eqn (44) are related to the locked long wave components

$$F_1=-\frac{i}{2}[-(\tilde\xi_T^1+\tilde\xi_R^1+\tilde\xi_1^L)+\tilde\xi_R^2+\tilde\xi_T^2+\tilde\xi_2^L]$$
$$(X=0) \qquad (56a)$$

$$F_2=-\frac{i}{2}[-(\tilde\xi_R^2+\tilde\xi_T^2+\tilde\xi_2^L)+\tilde\xi_T^3+\tilde\xi_3^L]$$
$$(X=L_1) \qquad (56b)$$

$$F_3=-\frac{1}{\Sigma_1}K_{1x}h_1(\psi_T^1-\psi_R^1)+\frac{1}{\Sigma_2}K_{2x}h_2(\psi_T^2-\psi_R^2)$$
$$+\frac{il_1}{16\sigma_1\Sigma_1}(b-R_1^+R_1^{-*})-\frac{il_2}{16\sigma_2\Sigma_2}$$
$$\times(T_2^+T_2^{-*}-R_2^+R_2^{-*}) \qquad (X=0) \qquad (56c)$$

$$F_4=-\frac{1}{\Sigma_2}K_{2x}h_2(\psi_D^L-\psi_E^L)+\frac{1}{\Sigma_3}K_{3x}h_3\psi_T^L$$
$$+\frac{il_2}{16\sigma_2\Sigma_2}(T_2^+T_2^{-*}-R_2^+R_2^{-*})-\frac{il_3}{16\sigma_3\Sigma_3}T_3^+T_3^{-*}$$
$$(X=L_1) \qquad (56d)$$

Once the incident wave groups and the geometrical parameters, including the current velocities, are described, the free long waves can be readily computed from eqn (54).

The coefficient matrix $\mathbf{N}$ in eqn (54) becomes singular when its determinant vanishes, i.e.:

$$\left[\frac{\Sigma_1}{\Sigma_3}(\lambda_2h_2)(\lambda_3h_3)+\frac{\Sigma_3}{\Sigma_1}(\lambda_2h_2)(\lambda_1h_1)\right]\cos 2\lambda_2L_1$$
$$-i\left[\frac{\Sigma_2^2}{\Sigma_1\Sigma_3}(\lambda_1h_1)(\lambda_3h_3)+\frac{\Sigma_1\Sigma_3}{\Sigma_2^2}(\lambda_2h_2)^2\right]$$
$$\times\sin 2\lambda_2L_1=0$$

or

$$\tan 2\lambda_2L_1$$
$$=-i\frac{(\lambda_2h_2)(\lambda_3h_3)(\Sigma_1\Sigma_2)^2+(\lambda_1h_1)(\lambda_2h_2)(\Sigma_2\Sigma_3)^2}{(\lambda_1h_1)(\lambda_3h_3)(\Sigma_2)^4+(\lambda_2h_2)^2(\Sigma_1\Sigma_3)^2} \qquad (57)$$

To satisfy this equation the necessary condition is that λ_2 must be real and λ_1 and λ_3 are imaginary, which represents the trapped modes in region 2. In the simpler situation where the conditions in region 3 are identical to those in region 1, i.e. $h_1=h_3$, $\lambda_1=\lambda_3$, and $\Sigma_1=\Sigma_3$, eqn (57) can be reduced to:

$$\tan 2\lambda_2L_1=-i\frac{2(\lambda_1h_1)(\lambda_2h_2)(\Sigma_1\Sigma_2)^2}{(\lambda_1h_1)^2\Sigma_2^4+(\lambda_2h_2)^2\Sigma_1^4} \qquad (58)$$

which can be solved for the nth eigenfrequency Ω for the resonance:

$$\Omega_n\beta_2L_1=\tfrac{1}{2}n\pi+\tan^{-1}\left[\frac{-i\beta_1h_1\gamma_2}{\beta_2h_2\gamma_1}\right] \qquad (59)$$

with:

$$\beta_j = \frac{\lambda_j}{\Omega} = \left[\frac{\gamma_j}{h_j} - \left(\frac{K_{1y}}{\Omega}\right)^2\right]^{1/2} \tag{60}$$

$$\gamma_j = \left(1 - \frac{K_{1y}V_j}{\Omega}\right)^2, \quad K_{1y} = \frac{\sin\alpha_1}{Cg_1}\Omega \tag{61}$$

and $j = 1, 2$. Because β_1 must be imaginary and β_2 must be real in eqn (59), one can derive the upper and the lower bounds of the incident wave angles within which the resonance of the trapped long waves might occur:

$$\frac{Cg_1}{V_1 + \sqrt{h_1}} < \sin\alpha_1 < \frac{Cg_1}{V_2 + \sqrt{h_2}} \tag{62}$$

As pointed out in the previous section, when λ_2 is zero, the solution in region 2 takes a different form, eqn (46). Applying the matching conditions (52) and (53), we obtain a different matrix equation for unknown coefficients, E_1, E_4, C_1 and C_2:

$$\mathbf{N}\begin{Bmatrix} E_1 \\ C_1 \\ C_2 \\ E_4 \end{Bmatrix} = \begin{Bmatrix} F_1 \\ F_2 \\ F_3 \\ F_4 \end{Bmatrix} \tag{63}$$

where the matrix $\mathbf{N}$ is given by

$$\mathbf{N} = \begin{Bmatrix} \Sigma_1 & 0 & -\Sigma_2 & 0 \\ 0 & \Sigma_2 L_1 & \Sigma_2 & -\Sigma_3 e^{2i\lambda_3 L_1} \\ -\dfrac{\lambda_1 h_1}{\Sigma_1} & \dfrac{ih_2}{2\Sigma_2} & 0 & 0 \\ 0 & -\dfrac{ih_2}{2\Sigma_2} & 0 & -\dfrac{\lambda_3 h_3}{\Sigma_3} e^{2i\lambda_3 L_1} \end{Bmatrix} \tag{64}$$

The right-hand side term of eqn (63) takes the same form as eqn (56). The determinant of eqn (64) is not zero. Therefore C_1 and C_2 are finite. There is no resonance at $\lambda_2 = 0$.

4 NUMERICAL EXAMPLES

Numerical examples for the diffraction of incident wave groups by different depth and current variations are discussed. In all calculations the wave amplitudes of the short wave components are assumed to be the same, i.e. $b = 1{\cdot}0$ in eqn (5). Moreover, the small parameter ϵ is chosen to be $0{\cdot}1$.

4.1 A 'top-hat' current

In the first example, the water depth is assumed to be uniform: $h_1 = h_2 = h_3$. The current velocity is confined within region 2. Defining the Froude number in a different region as

$$Fr_j = \frac{V_j}{(h_j)^{1/2}} \qquad (j = 1, 2, 3) \tag{65}$$

In the present case, $Fr_1 = Fr_3 = 0$, and $Fr_2 = \pm 0{\cdot}1$. The width of the jet-like current is $L/h_1 = 10$. The reflection and trapping of carrier (short) waves by the 'top-hat' current has been studied by Mei and Lo[15] and Kirby [16] in the shallow water limit. Using the parameters given above in the eigenfunction expansion method described in Section 2, the reflection and the transmission coefficients are calculated with different number of evanescent modes. A typical set of numerical solutions is shown in Table 1; the angle of incidence is $\pi/6$ and $k_1 h_1 = 1{\cdot}0$. It is clear that for this particular case the evanescent modes play an insignificant role. In the same table the reflection coefficient and the transmission coefficient for other geometries are also shown and will be discussed later.

In Fig. 2 the critical incident angles for the appearance of the caustics along the edges $X = 0$ and L_1 in the carrier waves and the wave envelope are shown for different $k_1 h_1$ with $Fr_2 = 0{\cdot}1$. Since the wave envelope has a longer wavelength and is refracted more by the current velocity, the corresponding critical incident angle is smaller. The present theory becomes invalid when the angle of incidence is larger than the critical angle for the wave group. In Fig. 3 the critical incident wave angles for the free long waves becoming decay modes in each region are shown. For the case

Table 1. Reflection and transmission coefficients with different numbers of evanescent modes (N); $\alpha_1 = \pi/6$ and $k_1 h_1 = 1{\cdot}0$

Description	$N = 0$	$N = 2$	$N = 4$	$N = 8$	$N = 16$
(*a*) *Reflection coefficient*					
'Top hat' current	0·015558	0·015260	0·015255	0·015254	0·015254
Forward step	0·002432	0·057786	0·061024	0·062222	0·062649
Backward step	0·164980	0·168898	0·169210	0·169306	0·169332
Shelf	0·256122	0·230487	0·229619	0·229352	0·229279
Trench	0·000970	0·065521	0·068493	0·068919	0·068988
(*b*) *Transmission coefficient*					
'Top hat' current	0·999879	0·999884	0·999884	0·999884	0·999884
Forward step	1·056230	1·054468	1·054265	1·054187	1·054159
Backward step	1·028587	1·027896	1·027840	1·027823	1·027818
Shelf	0·966644	0·973075	0·973281	0·973343	0·973361
Trench	1·000000	0·997851	0·997652	0·997622	0·997617

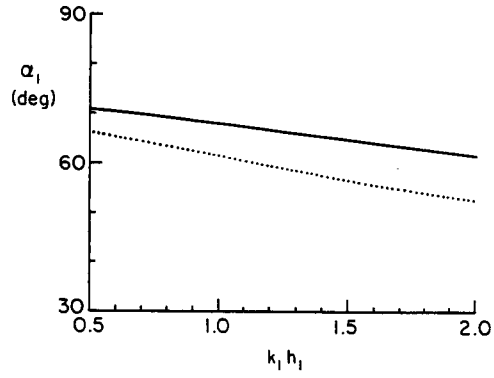

Fig. 2. The critical incident wave angles for carrier waves (——) and wave envelope (· · · · ·) for the case of a 'top hat' current; $Fr_2 = 0{\cdot}1$.

where the current flows in the same direction as the y-component of waves ($Fr = 0{\cdot}1$), the critical angles in region 1 are always greater than those in region 2. Equation (62) cannot be satisfied and the resonance of the trapped modes in region 2 does not exist. On the other hand, for the case with $Fr = -0{\cdot}1$, where the current flows against the direction of the y-component of wave propagation, the critical incident angles for the decay modes appearing in region 1 are smaller than those in the region 2. The trapped long waves can be resonated when the incident wave angles are between those two curves. The phenomena are further illustrated by plotting the free long wave amplitudes, $|E_2|$, for an angle of incidence $\alpha_1 = \pi/6$ (see Fig. 4). The resonant peak appears at $k_1 h_1 = 1{\cdot}5324$ for $Fr_2 = -0{\cdot}1$. The response, $|E_2|$, also becomes very large when $\lambda_2 = 0$ ($k_1 h_1 = 1{\cdot}3468$ and $1{\cdot}7234$ for $Fr_2 = 0{\cdot}1$ and $-0{\cdot}1$, respectively). This does not imply that a resonance has occurred as explained in Section 3. The corresponding resonance frequency, Ω_n, can be calculated from eqn

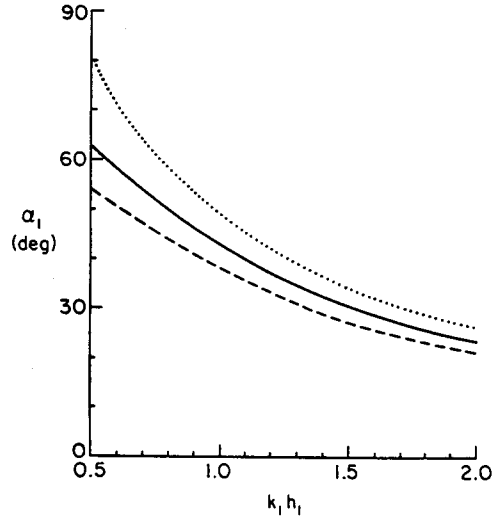

Fig. 3. The critical incident wave angles for the decay modes to appear in regions 1 and 2. (· · · · ·) region 2 with $Fr_2 = -0{\cdot}1$; (——) region 1 with $Fr_2 = \pm 0{\cdot}1$; (· · · · ·) region 2 with $Fr_2 = 0{\cdot}1$.

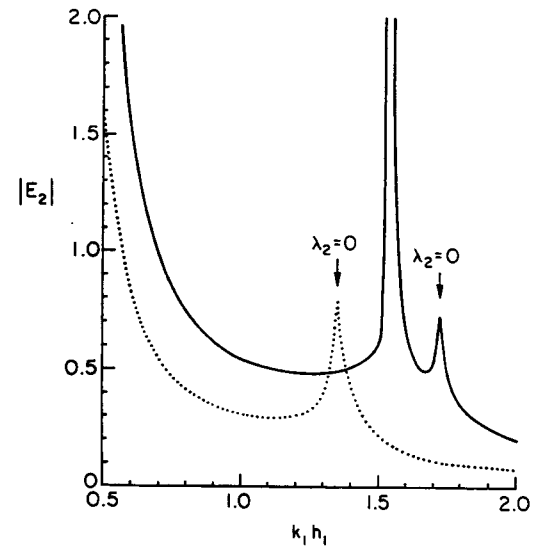

Fig. 4. The amplitudes of one of the free long wave components, $|E_2|$, over the 'top hat' current. The angle of incidence is $\pi/6$; (——) $Fr_2 = -0{\cdot}1$; (· · · · ·) $Fr_2 = 0{\cdot}1$.

(59) to be 0·6433. It should also be pointed out that the long wave amplitudes become quite large when the depth is small, where the Stokes wave theory breaks down.

4.2 A step without current

In the second example the authors examine the scattering of wave groups by a step, either a forward or a backward step, i.e. $h_i/h_2 <$ or > 1 with $h_2 = h_3$. In computing the reflection and the transmission coefficient for the carrier waves, a different number of evanescent modes has also been experimented. It is found, in general, that if 16 or more evanescent modes are used, the reflection and transmission coefficients remain practically the same. A typical set of results is shown in Table 1, with $k_1 h_1 = 1{\cdot}0$ and $\alpha_1 = \pi/6$. For the forward step $h_1 = h_2/2$ is used. In the case of the backward step $h_1 = 2h_2$ is employed. In the rest of the calculations reported herein 16 evanescent modes are used. In Fig. 5(a) the critical incident angles causing the decay modes for the free long waves in regions 1 and 2 are plotted for the forward step ($h_1 = h_2/2$) case. A similar set of curves is shown in Fig. 5(b) for the backward step ($h_1 = 2h_2$). In both cases the resonance of trapped modes does not exist, because the free long waves are allowed to propagate into infinity on the step. The second-order free long waves, $|E_1|$ and $|E_2|$, are plotted in Figs 6 and 7 for the incident wave angle $\alpha_1 = \pi/6$. In the case of the forward step, a local peak appears in $|E_1|$ and $|E_2|$, which corresponds to $\lambda_2 = 0$ ($k_1 h_1 = 0{\cdot}9278$), i.e the angle of incidence approaches the critical angles for the decay modes of the free long waves as shown in Fig. 5(a). For the backward step $\lambda_2 = 0$ corresponds to a value of $k_1 h_1$ which is larger than 2 and is outside of

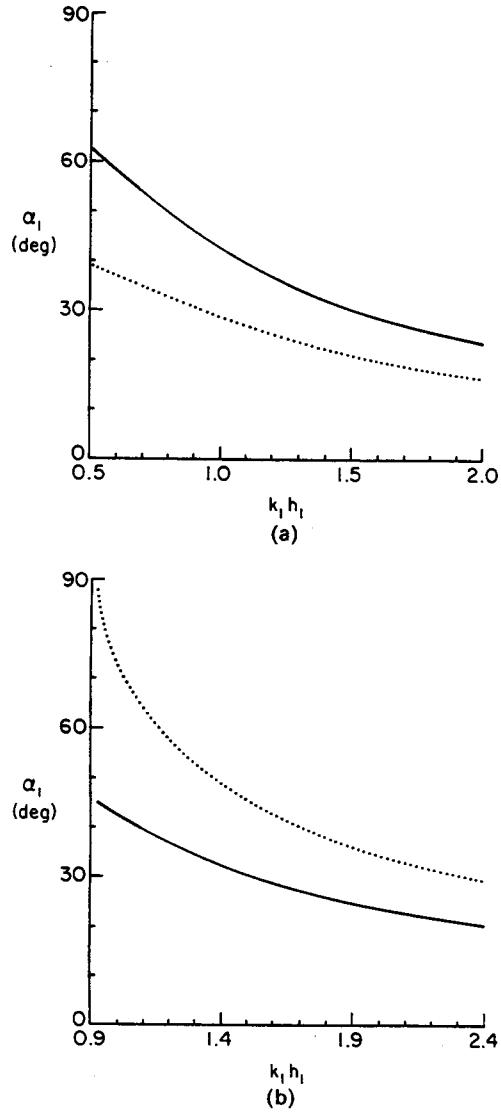

Fig. 5. The critical incident wave angles for the decay modes to appear in region 1 (——) and region 2 (· · · · ·): (a) a forward step, $h_1 = h_2/2$; (b) a backward step, $h_1 = 2h_2$.

the figure. For completeness, numerical results are also obtained for different depth ratios and angles of incidence with a fixed value of $k_1h_1 = 1{\cdot}0$ (see Fig. 8). It is interesting to observe that $|E_2|$ is relatively

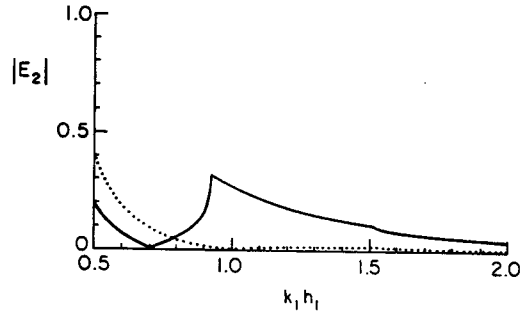

Fig. 6. The amplitudes of the free long waves, $|E_1|$, for the step cases with $\alpha_1 = \pi/6$ and $h_1 = h_2/2$ (forward step (——)) or $h_1 = 2h_2$ (backward step (· · · · ·).

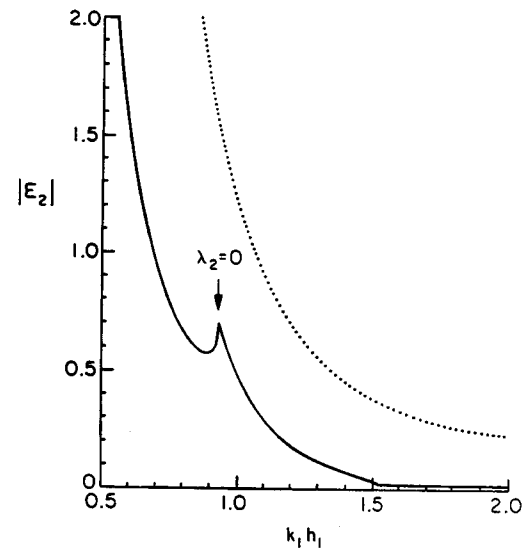

Fig. 7. The free long wave amplitude, $|E_2|$, for the step cases with $\alpha_1 = \pi/6$ and $h_1 = h_2/2$ (forward step (——)) or $h_1 = 2h_2$ (backward step (· · · · ·).

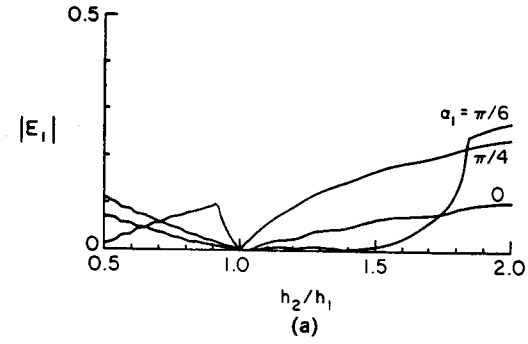

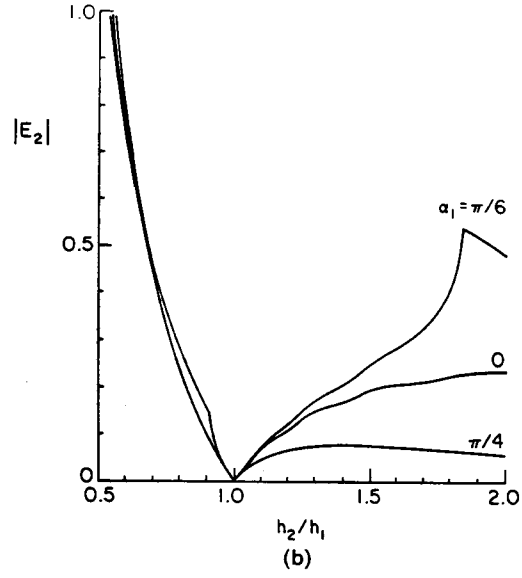

Fig. 8. The free long wave amplitudes $|E_1|$ and $|E_2|$ for the step cases with $k_1h_1 = 1{\cdot}0$. (a) $|E_1|$; (b) $|E_2|$.

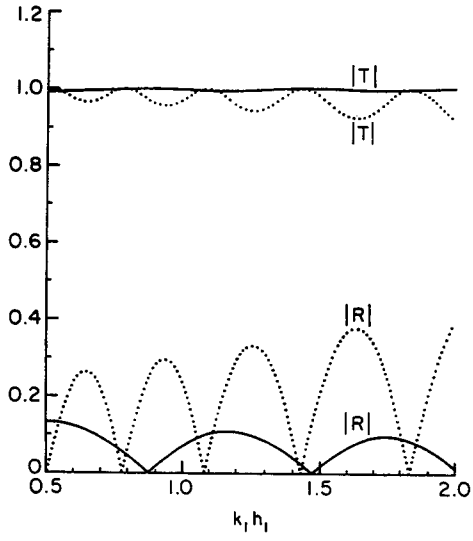

Fig. 9. Reflection and transmission coefficients of the carrier waves for both trench (——) and shelf (· · · · ·) cases. The angle of incidence is $\pi/6$.

insensitive to the angle of incidence in the case of a backward step.

4.3 A trench (or shelf) with currents

The last example concerns the generation and trapping of long waves over a trench or a shelf. In the case of a trench, the depth is fixed as $h_2 = 2h_1$ and $h_3 = h_1$. On the other hand, for the shelf the depth is $h_2 = 0{\cdot}5h_1$ and $h_3 = h_1$. In both situations $L = 10h_1$ and the current velocity is confined in region 2 with $Fr_2 = 0{\cdot}1$. The first-order reflection and transmission coefficients for both cases are plotted versus k_1h_1 in Fig. 9. To obtain these numerical solutions, 16 evanescent modes have been used (see Table 1). When the carrier waves propagate from a shallower depth to a deeper depth, caustics could appear if the angle of incidence is greater than a certain critical angle. In Fig. 10 these critical incident angles for the trench case are shown. For the present theory to be valid, the angles of incidence must be below both curves.

In Fig. 11 the critical incident wave angles for generating decay modes for free long waves in region 1 (or 3) and region 2 are shown for both trench and shelf

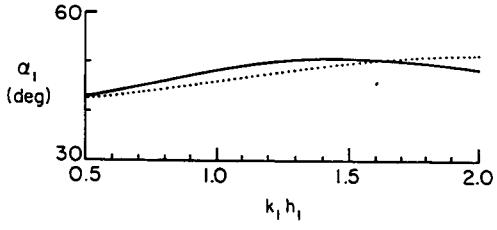

Fig. 10. The critical incident wave angles for caustics to appear in short waves (——) and wave envelope (· · · · ·) over a trench with $Fr_2 = 0{\cdot}1$.

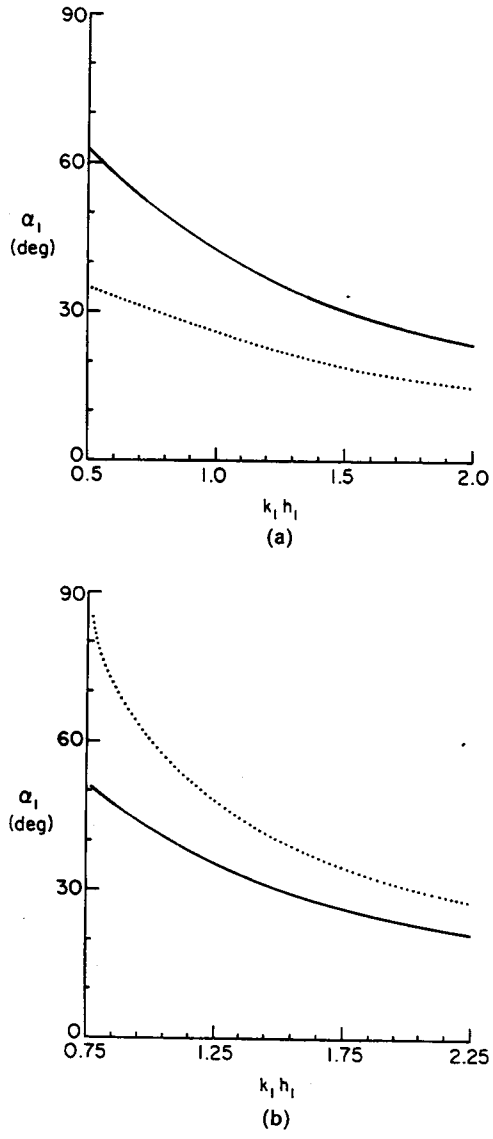

Fig. 11. The critical incident wave angles for the decay modes to appear in the region 1 (——) and region 2 (· · · · ·) of (a) a trench case and (b) a shelf case. In both cases $Fr_2 = 0{\cdot}1$.

cases. The trapped mode can be resonated in the shelf case when the incident wave angles are between the two curves shown in Fig. 11(b). One of the free long wave components in region 2, $|E_2|$, is plotted in Fig. 12 for both shelf and trench cases. The angle of incidence is fixed at $\pi/6$. From Fig. 11, the trapped long waves can be resonated for the shelf case when k_1h_1 is between 1·5 and 2·0. This is confirmed in Fig. 12; there is a resonance peak at $k_1h_1 = 1{\cdot}6066$. Note that $|E_2|$ also becomes very large when $L_2 = 0$ (or $k_1h_1 = 0{\cdot}7647$). Finally, the free long wave amplitudes, $|E_3|$, are shown for different angles of incidence in Fig. 13. Once again, the resonance occurs only for the shelf case within the range of angles of incidence, 37°–50° (see Fig. 11(b)). The precise incident angle is 39·42°. When the angle of incidence is greater than 50°, the long wave components on the shelf become decay modes and the amplitudes are small.

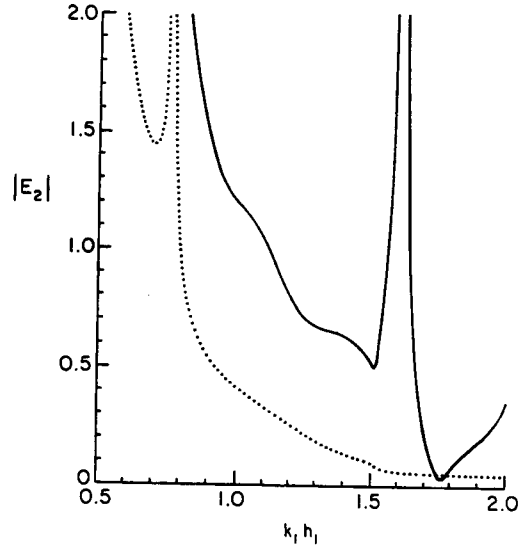

Fig. 12. The free long wave amplitudes, $|E_2|$, for both trench (· · · · ·) and shelf (——) cases with $Fr_2 = 0{\cdot}1$ and $\alpha_1 = \pi/6$.

5 CONCLUDING REMARKS

Analytical solutions for the forced and free long waves generated by the diffraction of short wave groups by abrupt changes in depth and current velocity are presented. Based on the mass conservation and the continuity of the second-order free surface displacement, a set of matching conditions for the second-order long waves along the edges of a trench (or a shelf) is developed. It is demonstrated that free long waves propagate with shallow-water speed, which is faster than the group velocity, and in a direction different from those of short waves and wave envelopes. The possibility for the resonance of trapped long waves is also confirmed. The analytical solutions presented herein can be used as bench-mark problems for future research.

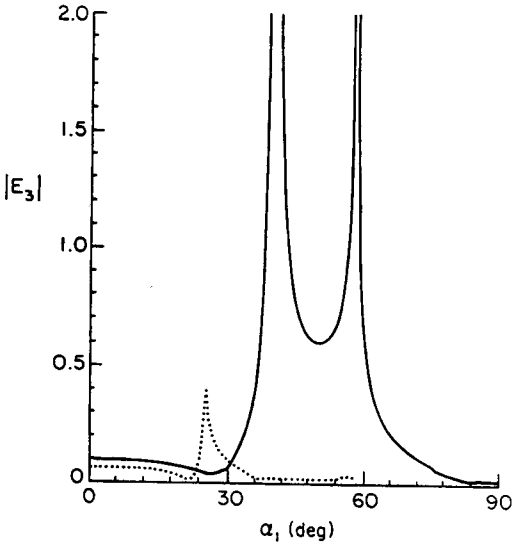

Fig. 13. The free long wave amplitudes, $|E_2|$, for both trench (· · · · ·) and shelf (——) cases with $Fr_2 = 0{\cdot}1$ and $k_1 h_1 = 1{\cdot}2$.

Carefully arranged laboratory experiments should be performed to verify the present second-order long wave generation theory for simple cases such as a step without current. The wave-maker must have the capability of generating incident locked long waves and being able to suppress the re-reflection of free long waves and the reflected locked long waves from the wave maker.[17]

For future research, a numerical model which can handle an arbitrary topography and current velocity field is needed for solving practical problems. The refraction, reflection and diffraction of the short waves should be included in the model. A numerical scheme must be developed for evaluating the forcing terms for the long waves. In the long wave model, the effect of bottom friction should be examined.

ACKNOWLEDGMENTS

The research presented here was initiated when the first author was visiting Delft Hydraulics and the Technical University of Denmark. The financial support provided by both institutions is appreciated. The research was also supported by the New York Sea Grant Institute and National Science Foundation through research grants (NA90AA-DSG078, BCS-8912579) to Cornell University.

REFERENCES

1. Molin, B., On the generation of long-period second-order free-waves due to changes in the bottom profile, Papers of the Ship Research Institute, Tokyo, Japan, 1982, No. 68.
2. Mei, C.C. & Benmousa, C., Long waves induced by short wave groups over an uneven bottom. *J. Fluid Mech.*, **139** (1984) 219–35.
3. Liu, P.L.-F., A note on long waves induced by short-wave groups over a shelf. *J. Fluid Mech.*, **205** (1989) 163–70.
4. Liu, P.L.-F., Dingemans, M.W. & Kostense, J.K., Long wave generation due to the reflection of short-wave groups over a shear current. *J. Phys. Oceanography*, **20** (1990) 53–9.
5. Bowers, E.C., Harbour resonance due to set-down beneath wave groups. *J. Fluid Mech.*, **79** (1977) 71–92.
6. Mei, C.C. & Agnon, Y. Long-period oscillations in a harbour by incident waves. *J. Fluid Mech.*, **208** (1989) 595–608.
7. Wu, J.K. & Liu , P.L.-F., Harbour excitations by incident wave groups. *J. Fluid Mech.*, **217** (1990) 595–613.
8. Symonds, G. & Bowen, A.J., The interaction of nearshore bars with incoming wave groups. *J. Geophys. Res.*, **89** (1984) 1953–9.
9. Roelvink, J.K. & Stive, M.J.F., Bar-generating cross-shore flow mechanism on a beach. *J. Geophys. Res.*, **94** (1989) 4785–800.
10. Agnon, Y. & Mei, C.C., Trapping and resonance of long shelf waves due to groups of short waves. *J. Fluid Mech.*, **195** (1988) 201–21.
11. Kirby, J.T., Dalrymple, R.A. & Seo, S.N., Propagation of obliquely incident water waves over a trench. Part 2. Current flowing along the trench. *J. Fluid Mech.*, **176** (1987) 95–116.

12. Evans, D.V., The transmission of deep-water waves across a vortex sheet. *J. Fluid Mech.*, **68** (1975) 389–401.
13. Agnon, Y. & Mei, C.C. Slow drift motion of a two-dimensional block in beam seas. *J. Fluid Mech.*, **151** (1985) 279–94.
14. Kirby, J.T., Propagation of weakly-nonlinear surface water waves in regions with varying depth and current. Tech. Report no. CE-83-37, Department of Civil Engineering, University of Delaware, Newark, DE, 1983.
15. Mei, C.C. & Lo, E., The effects of a jet-like current on gravity waves in shallow water. *J. Phys. Oceanography*, **14** (1984) 471–7.
16. Kirby, J.T., Comments on 'The effects of a jet-like current on gravity waves in shallow water,' *J. Phys. Oceanography*, **16** (1986) 395–7.
17. Kostense, J.K., Measurements of surf beat and set-down beneath wave groups. In *Proc. 19th Int. Conf. on Coastal Engg*, Houston, TX, 1984, pp. 724–740.